

# Coarse Graining in Block Copolymer Films

YOAV TSORI,<sup>1</sup> DAVID ANDELMAN<sup>2</sup>

<sup>1</sup>Department of Chemical Engineering, Ben Gurion University of the Negev, Beer Sheva 84105, Israel

<sup>2</sup>School of Physics and Astronomy, Raymond and Beverly Sackler Faculty of Exact Sciences, Tel Aviv University, Ramat Aviv, Tel Aviv 69978, Israel

Received 17 February 2006; revised 1 May 2006; accepted 26 May 2006

DOI: 10.1002/polb.20898

Published online in Wiley InterScience (www.interscience.wiley.com).

**ABSTRACT:** We present few ordering mechanisms in block copolymer melts in the coarse-graining approach. For chemically homogeneous or modulated confining surfaces, the surface ordering is investigated above and below the order–disorder temperature. In some cases, the copolymer deformation near the surface is similar to the copolymer morphology in bulk grain boundaries. Block copolymers in contact with rough surfaces are considered as well, and the transition from lamellae parallel to perpendicular to the surface is investigated as a function of surface roughness. Finally, we describe how external electric fields can be used to align block copolymer mesophases in a desired direction, or to induce an order–order phase transition, and dwell on the role of mobile dissociated ions on the transition. © 2006 Wiley Periodicals, Inc. *J Polym Sci Part B: Polym Phys* 44: 2725–2739, 2006

**Keywords:** block copolymers; confinement; electric fields; phase transitions

## INTRODUCTION

Block copolymers (BCPs) are heterogeneous polymers in which each polymer chain is composed of several chemically distinct homopolymer blocks, and connected together by a covalent bond. These polymeric systems exhibit fascinating structures in the nanometer scale, and can be created by self-assembly from solutions or the melt state.<sup>1,2</sup>

In addition, BCP are composite materials that have many applications. For example, by connecting together a stiff (rod-like) block with a flexible (coil) block, one can obtain a material which is rigid, but not brittle.<sup>3,4</sup> Moreover, the interplay between flexibility and toughness can be controlled by temperature. Different chain architecture (ring- or star-like) may lead to novel mechanical and flow properties.<sup>5</sup> In addition,

BCP have many industrial uses, because the length scales involved are smaller or comparable to the wavelength of light. These applications include waveguides, photonic band gap materials and other optoelectronic devices,<sup>6</sup> and dielectric mirrors.<sup>7</sup>

Our prime concern in this minireview are melts of BCP above the glass transition. However, it is worthwhile mentioning that BCP also exhibit interesting properties upon cooling below the glass transition into a solid state. Some BCP may undergo crystallization of one or more components that is accompanied by strong structural changes, while other BCP systems stay in the vitrified state upon cooling.

In the molten state, because of competition between enthalpy and entropy, at high temperatures, the BCP melt behaves as a disordered fluid, while at low temperatures the macroscopic phase separation is hindered, because two (or more) immiscible subchains cannot be detached from each other, as they try to phase-separate due to block incompatibility. Hence, BCPs phase-separate

Correspondence to: D. Andelman (E-mail: andelman@post.tau.ac.il)

*Journal of Polymer Science: Part B: Polymer Physics*, Vol. 44, 2725–2739 (2006)  
© 2006 Wiley Periodicals, Inc.

into a variety of micro-ordered structures, with their characteristic size depending on the BCP chain length and other system parameters.<sup>1,2</sup> The morphology and structure of the prevailing phase depend on the lengths of constituent subchains (also called blocks), the chemical interactions between the blocks, the temperature, and the chain architecture. The BCP microdomain size ranges from about 10 to several 100 nm.

A typical example of a well-studied di-BCP, polystyrene–polyisoprene (PS-PI), is shown in Figure 1.<sup>8</sup> As temperature is kept cool below the order–disorder temperature (ODT), the disorder melt of chains microphase separates into one of the mesophases: lamellar, hexagonal, body centered cubic (bcc), or gyroid.

The present paper reviews several mechanisms that can be used to achieve a desired ordering and orientation in thin films of BCP. By no means

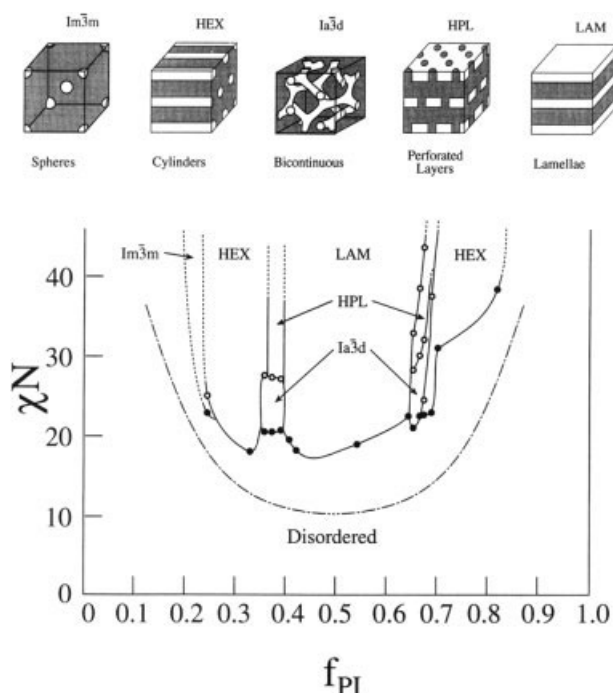


**Figure 1.**  $\chi N$  versus  $f_{PI}$  phase diagram for PS-PI diblock copolymers. The dash-dot curve is the mean field prediction for the ODT. Solid curves have been drawn to delineate the different phases observed, but might not correspond to precise phase boundaries. Five different ordered microstructures (shown schematically) have been observed for this chemical system. Reproduced from Khandpur, A. K.; Foerster, S.; Bates, F. S.; Hamley, I. W.; Ryan, A. J.; Bras, W.; Almdal, K.; Mortensen, K. *Macromolecules* 1995, 28, 8796, with permission from American Chemical Society, © 1995 American Chemical Society.

is this an exhaustive review; for more thorough reviews on the subject, including other mechanisms to control BCP morphology, such as shear flow, nonlamellar morphologies, and disparate Kuhn lengths of the two polymer blocks, interested readers may turn to refs. 9–11, and recent reviews by Thomas and coworkers<sup>12</sup> and Bucknall,<sup>13</sup> and references therein. The outline of our paper is as follows: A simple analytical model, valid in the weak segregation limit (WSL), is presented in The Model section. In the next section, we considered BCPs above the ODT point and in contact with chemically patterned surfaces. The polymer density is given as a function of a predesigned and frozen chemical pattern on the surface. Thin films of di-BCPs below the ODT confined between two flat and parallel surfaces are investigated in the subsequent section. We find that, for a one-dimensional chemical surface pattern, the lamellae are tilted with respect to the parallel surfaces. If the surface and lamellar periodicities are equal, the lamellae are formed perpendicular to the surfaces. We relate the orientation phenomenon to the formation of tilt boundary (chevrons) defects in bulk lamellar phases. Beside chemically heterogeneous surfaces, rough surfaces are investigated in the subsequent section. A simple explanation to the parallel to perpendicular transition in these BCPs systems as function of surface roughness is proposed. Alignment of confined lamellae by external electric fields is studied in BCPs in the following section. It is shown that, because different polymers have different values of the dielectric constant, the electrostatic energy favors an orientation of lamellae in a direction perpendicular to the confining electrodes. This electrostatic tendency can be used to overcome interfacial interactions with the bounding electrodes and align structures in a desired direction.

## THE MODEL

We start by defining the order parameter,  $\phi(\mathbf{r}) \equiv \phi_A(\mathbf{r}) - f$ , as the local deviation of the A monomer concentration from its average. The bulk free energy can be expressed as an expansion in  $\phi(\mathbf{r})$  in WSL and is written as follows:<sup>14,15</sup>

$$\frac{Nb^3F_b}{k_B T} = \int \left\{ \frac{1}{2} \tau \phi^2 + \frac{1}{2} h (\nabla^2 \phi + q_0^2 \phi)^2 + \frac{1}{6} \Lambda \phi^3 + \frac{u}{24} \phi^4 \right\} d^3 r \quad (1)$$

The parameter  $\tau = 2\rho N(\chi_c - \chi)$  measures the distance from the critical point ( $\tau = 0$ ) in terms of the Flory parameter  $\chi \sim 1/T$ . At the critical point (or equivalently the ODT),  $\chi_c \simeq 10.49/N$ .  $d_0 = 2\pi/q_0$  is the fundamental periodicity in the system, and is expressed by the polymer radius of gyration  $R_g$ , through  $q_0 \simeq 1.95/R_g$ . The Kuhn statistical segment length,  $b$ , is taken here to be equal for the two polymer blocks.<sup>11</sup> In addition,  $h = 1.5\rho c^2 R_g^2/q_0^2$ , the chain density per unit volume is  $\rho = 1/Nb^3$ , and  $\Lambda$  and  $u$  are, respectively, the three- and four-point vertex functions, calculated by Leibler.<sup>14</sup>

For simplicity, we will restrict most (but not all) of the discussion below to lamellar phases of symmetric BCPs. This allows us to simplify the aforementioned free energy by considering only the symmetric case:  $f = \frac{1}{2}$ , where the cubic  $\Lambda$ -dependent term drops out. When we treat the bcc to hexagonal transition, we will consider also the cubic term in the free energy, as it is indispensable to describe asymmetric phases.

The earlier discussed free-energy functional, eq 1, and similar forms<sup>16,17</sup> have been used successfully by other authors in the past, to describe BCPs<sup>18–22</sup> and other systems with spatially modulated phases.<sup>23</sup> The free energy, eq 1, describes a system in the disordered phase having a uniform  $\phi = 0$  for  $\chi < \chi_c$  (positive  $\tau$ ), while for  $\chi > \chi_c$  (negative  $\tau$ ), the system is in the lamellar phase for  $f = \frac{1}{2}$ , and  $\Lambda = 0$ , and can be described approximately by a single  $q$ -mode  $\phi = \phi_L \exp(i\mathbf{q}_0 \cdot \mathbf{r})$ , with modulation amplitude given by  $\phi_L^2 = -8\tau/u$ . The validity of eq 1 is limited to the WSL region of the phase diagram. It is close enough to the critical point, where the expansion in powers of  $\phi$  and its derivatives is valid, but not too close to it, because the critical fluctuations become important.<sup>24,25</sup>

## DISORDERED BCPs IN CONTACT WITH CHEMICALLY PATTERNED SURFACES

When the BCP melt is in contact with a chemically heterogeneous but otherwise flat surface, the surface free energy has the form

$$F_s = \int \sigma(\mathbf{r}_s) \phi(\mathbf{r}_s) d^2 \mathbf{r}_s + \text{const.} \quad (2)$$

The surface field is  $\sigma(\mathbf{r}_s) \equiv \gamma_{AS} - \gamma_{BS}$ , where  $\gamma_{AS}$  and  $\gamma_{BS}$  are the interfacial interactions of the A and B blocks with the surface, respectively, and the integration is carried out over the position of the confining surfaces parameterized by the vector  $\mathbf{r}_s$ .

Preferential adsorption of the A block ( $\phi > 0$ ) onto the surface is modeled by a constant  $\sigma < 0$  surface field, resulting in parallel-oriented layers (a perpendicular orientation of the chains). One way of producing such a surface field in experiments is to coat the substrate with random copolymers.<sup>26,27</sup> If the pattern is spatially modulated,  $\sigma(\mathbf{r}_s) \neq 0$ , then the A and B blocks are attracted to different regions of the surface.

## One Surface

Consider first BCPs confined by one surface located at  $y = 0$ , as is depicted in Figure 2(a). A generalization to two parallel surfaces is not difficult and will be given later. The surface chemical pattern  $\sigma(\mathbf{r}_s) = \sigma(x, z)$  can be decomposed in terms of its  $q$ -modes

$$\sigma(x, z) = \sum_{\mathbf{q}} \sigma_{\mathbf{q}} e^{i(q_x x + q_z z)} \quad (3)$$

where  $\mathbf{q} = (q_x, q_z)$ , and  $\sigma_{\mathbf{q}}$  is the mode amplitude. Similarly,  $\phi$  can be written as a sum

$$\phi(\mathbf{r}) = \sum_{\mathbf{q}} \phi_{\mathbf{q}}(y) e^{i(q_x x + q_z z)} \quad (4)$$

Close to the ODT, the free energy is stable to second order in  $\phi$ , and higher order terms (i.e., the  $\phi^4$  term) can be neglected. Then  $\phi(\mathbf{r})$  is inserted into eq 1 and an integration over the  $x$  and  $z$  coordinates is carried out. Minimization with respect to  $\phi_{\mathbf{q}}(y)$  yields the Euler–Lagrange equation<sup>28,29</sup>

$$[\tau/h + (q^2 - q_0^2)^2] \phi_{\mathbf{q}} + 2(q_0^2 - q^2) \phi_{\mathbf{q}}'' + \phi_{\mathbf{q}}'''' = 0 \quad (5)$$

Note that the equation is linear and that the Fourier harmonics  $\phi_{\mathbf{q}}$  are not coupled. The solution is a sum of exponentials,

$$\phi_{\mathbf{q}}(y) = A_{\mathbf{q}} \exp(-k_{\mathbf{q}} y) + B_{\mathbf{q}} \exp(-k_{\mathbf{q}}^* y) \quad (6)$$

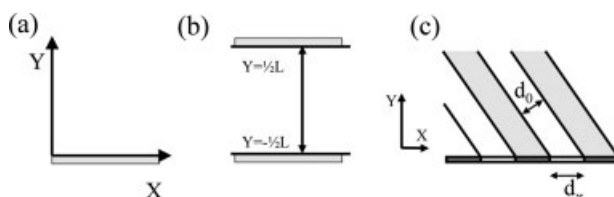


**Figure 2.** Schematic illustration of the coordinate system for BCPs confined by one [part (a)] or two [part (b)] planar and parallel surfaces. (c) Lamellae are formed tilted with respect to the surface if the surface periodicity  $d_x$  is larger than the natural one  $d_0$ .

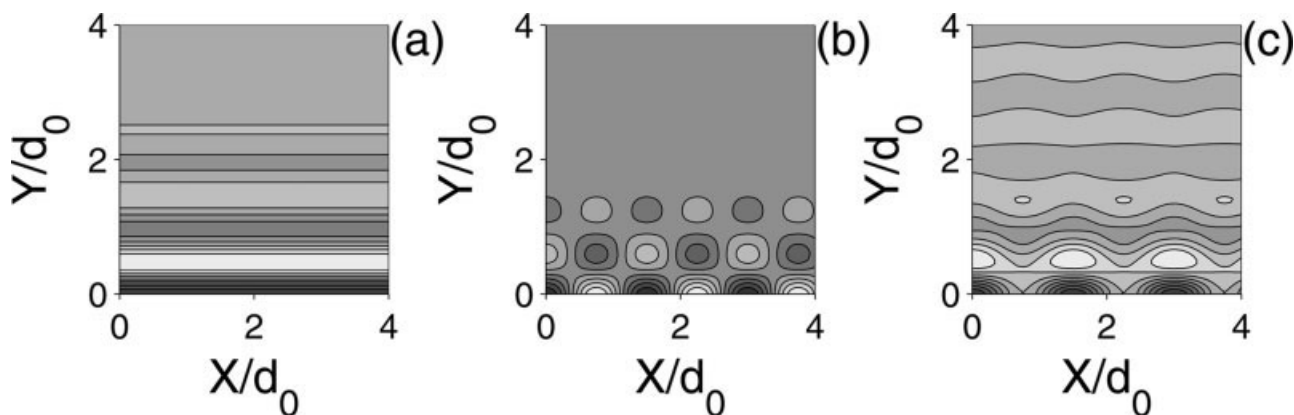


**Figure 3.** A BCP melt confined by one surface at  $y = 0$ . B-monomer density is high in dark regions, while A monomers are in light regions. In (a) the surface is uniform,  $\sigma = 0.3$  and in (b) it has stripes given by  $\sigma = 0.3 \cos(\frac{2}{3}q_0x)$ . The “combined” effect is shown in part (c) where  $\sigma = 0.3 + 0.3 \cos(\frac{2}{3}q_0x)$  has a uniform and modulated part. The Flory parameter is  $N\chi = 10.2$ , and lengths in the  $x$  and  $z$  directions are scaled by the lamellar period  $d_0$ . Reproduced from Tsori, Y.; Andelman, D. *Interface Sci* 2003, 11, 259, with permission from Springer.

where the modulation constant  $k_q$  and the amplitude  $A_q$  are given by

$$\begin{aligned} k_q^2 &= q^2 - q_0^2 + i\sqrt{\tau/h} \\ A_q &= -\sigma_q \left( 2\text{Im}(k_q)\sqrt{\tau h} \right)^{-1} \end{aligned} \quad (7)$$

In Figure 3, we give examples of the polymer morphologies in the case of three simple, surface patterns. A uniform surface [in (a),  $\sigma = \sigma_0$  is constant] causes exponentially decaying density modulations to propagate in the  $y$ -direction. A striped surface [in (b),  $\sigma = \sigma_q \cos(qx)$ ] creates

a disturbance that is periodic in the  $x$ -direction, which decays exponentially in the  $y$ -direction. The combined surface pattern [in (c),  $\sigma = \sigma_0 + \sigma_q \cos(qx)$ ] induces density modulations which are the sum of the ones in (a) and (b).

In Figure 4(a), we show a chemical pattern consisting of V-shaped stripes on the  $y = 0$  surface. The polymer density in parallel planes with increasing distance from the surface is shown in (b) and (c). Note how the frustration induced by the tips of surface chemical pattern [in (a)] is relieved, as the distance from the surface increases. Similar morphology is observed when

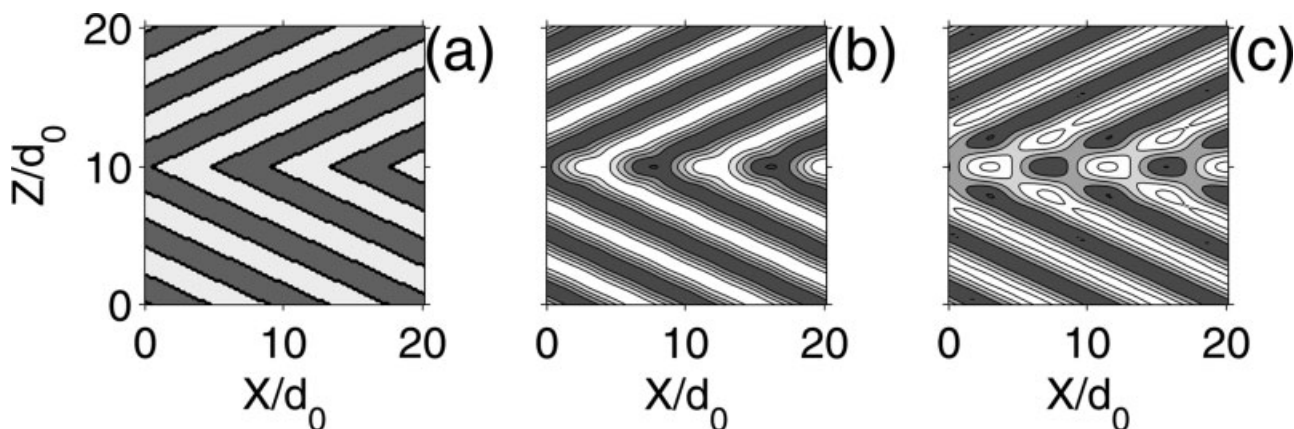


**Figure 4.** Propagation of surface pattern into the bulk. The surface pattern in the  $y = 0$  plane is shown in (a), where white (black) show regions preferring A (B) monomers. Parts (b) and (c) are contour plots of the polymer density at  $y = 3d_0$  and  $y = 8d_0$ , respectively. The Flory parameter is  $N\chi = 9.5$ . Reproduced from Tsori, Y.; Andelman, D. *Interface Sci* 2003, 11, 259, with permission from Springer.

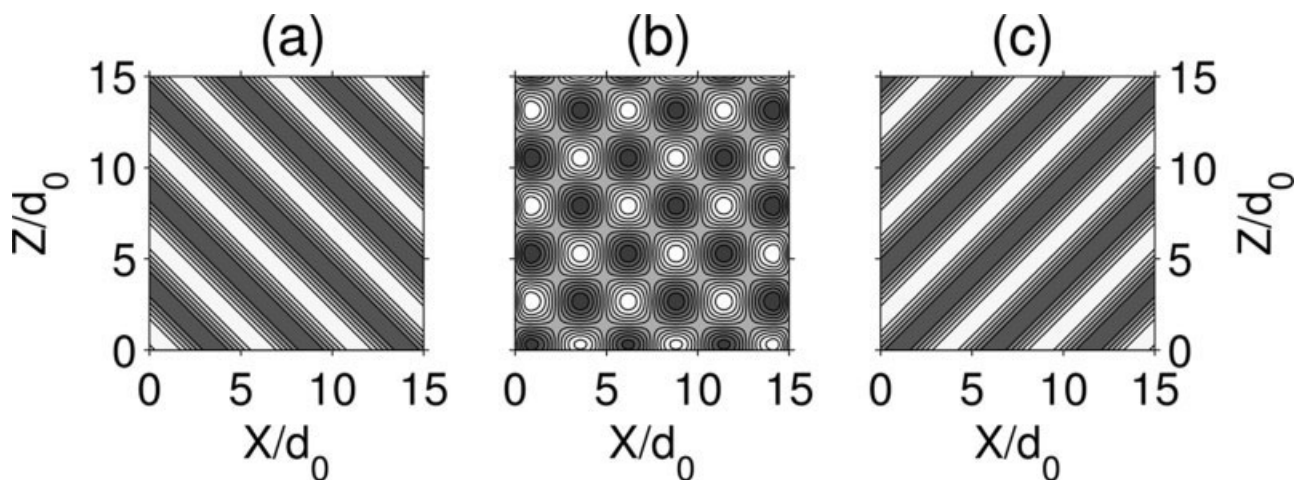


**Figure 5.** BCP melt confined by two flat parallel striped surfaces, depicted in parts (a) and (c), and located at  $y = -d_0$  and  $y = d_0$ , respectively. The melt morphology in the mid-plane ( $y = 0$ ) is shown in part (c). The Flory parameter is  $N\chi = 9$ . Reproduced from Tsori, Y.; Andelman, D. *Macromolecules* 2001, 34, 2719, with permission from American Chemical Society, © 2001 American Chemical Society.

two grains of lamellar phase meets with a tilt angle, creating a tilt grain boundary in bulk systems.<sup>30</sup>

### Two Confining Surfaces

The case of a BCP confined by two flat parallel surfaces<sup>29</sup> follows as a straightforward generalization, because the behavior is still governed by eq 5. Figure 5 shows how two simple surface patterns can be used to achieve a complex three-dimensional polymer morphology, even though the melt is in its bulk-disordered phase. The stripes on the two surfaces are rotated by 90° with respect to each other. A symmetric “checkerboard” morphology appears in the mid-plane.

Up to this point, the BCP melt was assumed to be in its bulk-disordered phase (above the bulk ODT point). When a melt in the lamellar phase (below ODT) is confined in a thin film, the morphology is dictated by a complex interplay between the natural periodicity and the imposed film thickness.

### LAMELLAR BCP BETWEEN TWO CHEMICALLY PATTERNED SURFACES

We now turn to describe BCPs below the ODT temperature, in the lamellar phase, confined by one or two surfaces. The phase behavior of thin BCP films in the lamellar phase subject to *uniform* surface

fields has been investigated experimentally<sup>31</sup> and theoretically,<sup>32–38</sup> and was found to consist of parallel, perpendicular, and mixed lamellar phase. The latter phase has parallel lamellae extending from one surface, which are jointed in a T-junction defect, with perpendicular lamellae extending from the opposite surface.<sup>39,40</sup> At a given inter-surface spacing, increasing the (uniform) surface interactions promotes a parallel orientation with either A-type or B-type monomers adsorbed onto the surface. However, if the spacing  $L$  between the surfaces is incommensurate with the lamellar periodicity, or the incompatibility  $\chi$  is increased, a perpendicular orientation is favored.<sup>41</sup>

In the treatment given later, a new effect can be observed when the surfaces are taken to be nonuniform, “striped”, with regions of alternating preferences to the A and B blocks [Fig. 2(c)].<sup>42</sup> The stripe periodicity  $d_x$  is assumed to be larger than the natural (bulk) periodicity,  $d_x > d_0$ , and the stripes are modeled by

$$\sigma(x, z) = \sigma_q \cos(q_x x) \quad (8)$$

and are translational invariant in the  $z$ -direction. The surface  $q$ -mode is  $q_x = 2\pi/d_x < q_0$  and the lamellae tilt angle  $\theta$  is defined as  $\arccos(d_0/d_x)$ .

Contrary to the system above the ODT, a linear response theory assuming small order parameter as a response to the surface field is inadequate here, since the bulk phase has an inherent spatially varying structure.

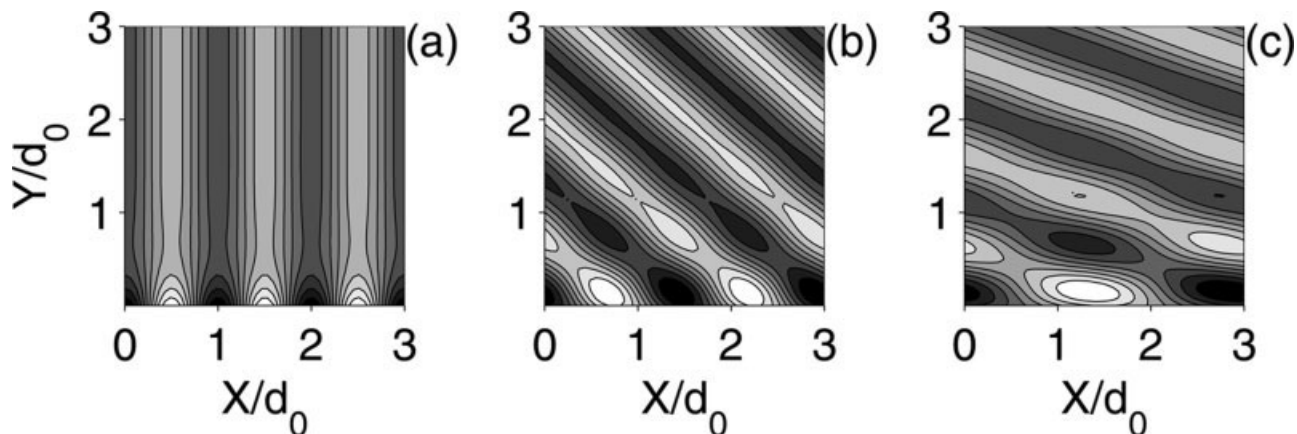


**Figure 6.** Tilted lamellar phase in contact with one patterned surface at  $y = 0$ . [See also Fig. 2(c)]. The surface patterning is modeled by the term  $\sigma_q \cos(2\pi x/d_x)$ . The lamellae tilt angle  $\theta = \arccos(d_0/d_x)$  increases as the periodicity of the surface  $d_x$  increases:  $\theta = 0$  for  $d_x = d_0$  in (a),  $\theta \simeq 48.1^\circ$  for  $d_x = \frac{3}{2}d_0$  in (b) and  $\theta \approx 70.5^\circ$  for  $d_x = 3d_0$  in (c). In the plots  $\sigma_q/hq_0^3\phi_L = 1$ . The Flory parameter  $N\chi = 11.5$  and a surface Flory parameter is chosen here as in ref. 43. Reproduced from Tsori, Y.; Andelman, D. *J Chem Phys* 2001, 115, 1970, with permission from American Institute of Physics.

The surface effects are contained in the correction to the order parameter

$$\delta\phi(\mathbf{r}) \equiv \phi(\mathbf{r}) - \phi_b(\mathbf{r}) \quad (9)$$

where  $\phi_b$  is a “tilted” bulk lamellar phase given by

$$\phi_b = -\phi_L \cos(q_x x + q_y y) \quad (10)$$

$$q_x = q_0 \cos \theta, \quad q_y = q_0 \sin \theta, \quad (11)$$

The bulk ordering is depicted schematically as tilted lamellae in Figure 2(c). For the correction order parameter  $\delta\phi$ , we choose

$$\delta\phi(x, y) = g(y) \cos(q_x x). \quad (12)$$

This correction describes a lamellar ordering perpendicular to the surface, and commensurate with its periodicity  $d_x = 2\pi/q_x$ . The overall morphology of the lamellae is a superposition of the correction field  $\delta\phi$  with the tilted bulk phase, having a periodicity  $d_0$ . The region where the commensurate correction field  $\delta\phi$  is important is dictated by the amplitude function  $g(y)$ . The total free energy  $F = F_b + F_s$  is now expanded about its bulk value  $F[\phi_b]$  to second order in  $\delta\phi$ . The variational principle with respect to  $g(y)$  yields a master equation:

$$[A + C \cos(2q_y y)]g(y) + Bg''(y) + g''''(y) = 0, \quad (13)$$

with parameters  $A$ ,  $B$ , and  $C$  given by

$$A = -\tau/h + q_y^4, \quad B = 2q_y^2, \quad C = -\tau/h. \quad (14)$$

The results for a melt confined by one sinusoidally patterned surface,  $\sigma(x) = \sigma_q \cos(q_x x)$ , are shown in Figure 6, for several values of surface periodicity  $d_x$  and for fixed value of the Flory parameter  $\chi > \chi_c$ . There is no average preference to one of the blocks,  $\langle \sigma \rangle = 0$ . The main effect of increasing the surface periodicity  $d_x$  with respect to  $d_0$  is to stabilize tilted lamellae, with increasing tilt angle. Note that even for  $d_x = d_0$  [Fig. 6(a)] yielding no tilt, the perpendicular lamellae have a different structure close to the surface, as is induced by the surface pattern. Although the surface interactions are assumed to be strictly local, the connectivity of the chains causes surface-bound distortions to propagate into the bulk of the BCP melt. In particular, this is a strong effect in the weak-segregation regime we are considering.

So far, in this section, we have considered the semi-infinite problem of a BCP melt confined by one patterned surface. It is of experimental and theoretical interest to study thin films of BCPs when they are confined between a heterogeneous (patterned) surface and a second chemically homogeneous surface. This situation is encountered when a thin BCP film is spread on a patterned surface. The second interface is the film/air interface and is homogeneous. Usually, the free surface has a lower surface tension with one of the two blocks. This bias can be modeled by adding a constant  $\sigma_0$  term to the  $\sigma(x)$  surface field. For simplicity, we assume that the surface at  $y = -\frac{1}{2}L$  has purely sinusoidal stripes, while at  $y = \frac{1}{2}L$  the surface is

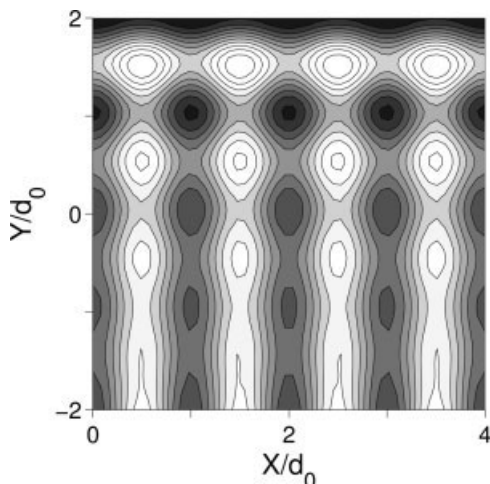


**Figure 7.** A BCP-confined film showing a crossover from perpendicular lamellae at the  $y = -\frac{1}{2}L = -2d_0$  surface to parallel lamellae at the other surface,  $y = \frac{1}{2}L$ . The pattern on the bottom surface,  $\sigma(x) = \sigma_q \cos(q_0 x)$ , has the bulk periodicity  $d_0$ , and amplitude  $\sigma_q = 2hq_0^3$ , while the top surface ( $y = \frac{1}{2}L$ ) is homogeneously attractive to the B polymer (in black),  $\sigma_0 = 4hq_0^3$ . The Flory parameter is given by  $N\chi = 10.7$ . Reproduced from Tsoi, Y.; Andelman, D. *J Chem Phys* 2001, 115, 1970, with permission from American Institute of Physics.

attractive to one of the A/B blocks with a constant preference:

$$\begin{aligned} \sigma(x) &= \sigma_q \cos(q_x x), & \text{at } y = -\frac{1}{2}L, \\ \sigma(x) &= \sigma_0, & \text{at } y = \frac{1}{2}L. \end{aligned} \quad (15)$$

A neutral surface at  $y = \frac{1}{2}L$  is obtained as a special case with  $\sigma_0 = 0$ . The eq 10 for the bulk-tilted phase is modified ( $y \rightarrow y + \frac{1}{2}L$ ) in order to match the stripe surface pattern at  $y = -\frac{1}{2}L$ ,

$$\phi_b = -\phi_L \cos \left[ q_x x + q_y \left( y + \frac{1}{2}L \right) \right] \quad (16)$$

The homogeneous surface field at  $y = \frac{1}{2}L$  induces a lamellar layering parallel to the surface, since the two A/B blocks are covalently linked together. The simplest way to account for this layering effect is to include an  $x$ -independent term  $w(y)$  in our *ansatz*, eq 12, for the order parameter:

$$\delta\phi(x, y) = g(y) \cos(q_x x) + w(y). \quad (17)$$

*Tilted* lamellar phases may appear when the BCP is confined by one homogeneous and a second patterned surface, if the surface imposed periodicity  $d_x$  is equal or larger than the bulk periodicity

$d_0$ . A “T-junction” morphology, occurring as a special case when the surface periodicity is equal to the bulk period, is shown in Figure 7, where perpendicular lamellae are seen to extend from the patterned surface. The homogeneous field at the opposite surface favors a parallel orientation of the lamellae. The crossover region between the two orientations is found in the middle of the film, and its morphology depends on temperature (the  $\chi$  parameter). The effect of the homogeneous field is evident, as parallel ordering extends from the top surface. We see here that strong enough modulated surface fields stabilize the tilted lamellar phases and, in particular, the mixed phase.

### BCPs IN CONTACT WITH ROUGH SURFACES

In the preceding sections, we have described how the copolymer morphology is influenced by chemically homogeneous or patterned surfaces that are smooth and flat. Another way to control BCP structure is by the use of rough or corrugated surfaces. This method has some advantages, because it is rather straightforward to construct experimentally such surfaces.<sup>44</sup> When a lamellar stacking is placed parallel to a rough, sinusoidally modulated surface (Fig. 8), the lamellar state is a compromise between interfacial interactions preferring that the lamellae closely follow the surface contour, and bending and compression energies preferring flat layers.

The surface roughness is modeled by a single one-dimensional corrugation mode, whose height in the  $z$ -direction above an  $(x, y)$  reference plane is given by  $h(x) = R \cos(q_s x)$ .  $q_s$  and  $R$  are the wavenumber and amplitude of the surface roughness, respectively (Fig. 8). The BCP is put above

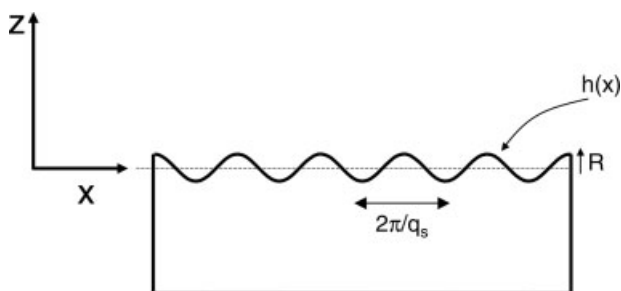


**Figure 8.** Schematic illustration of a rough surface, with sinusoidal height undulations  $h(x) = h_0 + R \cos(q_s x)$ .

the substrate in the half-space  $z \geq h(x)$ . We denote  $\gamma_{AB}$  as the interfacial interaction between the A and B blocks in the polymer chain.

For lamellae oriented perpendicular to the surface, the order parameter is written as<sup>44</sup> follows:

$$\phi_{\perp}(\mathbf{r}) = \phi_0 \cos(q_0 x + q_0 u(x, z)) \quad (18)$$

The function  $u(x, z)$  describes the surface-induced deviation of the A/B interface from its flat (perfect) shape. The bulk part of the free energy can be written as<sup>45-47</sup> follows:

$$F_b = \frac{1}{2} \int [K(u_{zz})^2 + B(u_x)^2] d^3 r \quad (19)$$

where  $u_x = \partial u / \partial x$ ,  $u_{zz} = \partial^2 u / \partial z^2$ ,  $K \sim d_0 \gamma_{AB}$  is the bending modulus and  $B \sim \gamma_{AB} / d_0$  is the compression modulus. To the elastic energy integral given earlier must be added a term taking into account the interfacial energies of the A and B blocks. This is simply given by  $\frac{1}{2}(\gamma_{AS} + \gamma_{BS})$ , multiplied by a correction factor. This factor is  $1 + \frac{1}{4}(q_s R)^2$ , reflecting the fact that the real surface area is larger than the projected one, and assuming small roughness  $q_s R \ll 1$ . Minimization of the free energy given earlier gives the expression for  $u$ . The deformation  $u$  is larger close to the surface, as can be seen from the deformation of the perpendicular lamellae in Figure 9(a).

Substitution of the expression for  $u$  back into the free-energy integral eq 19 gives the free energy per unit area of the perpendicular lamellae

$$F_{\perp} \simeq \phi_0^2 \frac{(\gamma_{AS} - \gamma_{BS})^2}{q_0 K} + \frac{1}{2}(\gamma_{AS} + \gamma_{BS}) \left( 1 + \frac{1}{4}(q_s R)^2 \right) \quad (20)$$

The deformation  $u$  for parallel lamellae can be achieved in a similar way. The resulting parallel layering is seen in Figure 9(b), with the same parameters as in part (a). The total free energy in this case is given as follows:

$$F_{\parallel} \simeq \phi_0^2 \frac{(\gamma_{AS} - \gamma_{BS})^2}{q_0 K} \left( \frac{q_0}{q_s} \right)^2 (q_0 R)^2 + \left[ \left( \frac{1}{2} - \phi_0 \right) \gamma_{AS} + \left( \frac{1}{2} + \phi_0 \right) \gamma_{BS} \right] \left( 1 + \frac{1}{4}(q_s R)^2 \right) \quad (21)$$

Here again, we find the same factor  $1 + \frac{1}{4}(q_s R)^2$ , but the energies of interaction with the surface are different from the previous case: the A and B polymers do not cover the surface equally, and hence

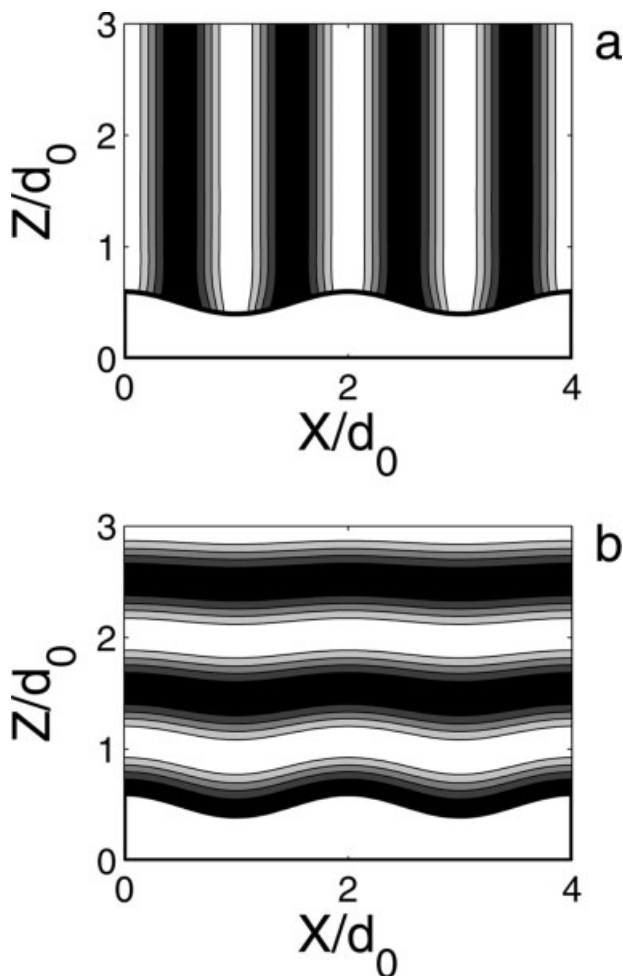


**Figure 9.** Perpendicular (a) and parallel lamellae (b) on rough surfaces. The lamellar periodicity is half the surface one. The parameter used are  $B = 2 \times 10^5 \text{ J/m}^2$ ,  $K = B/(4q_0^2)$  and  $\sigma = \gamma_{AS} - \gamma_{BS} = \sqrt{BK}/4$ . Reproduced from Tsori, Y.; Andelman, D. *Macromolecules* 2003, 36, 8560, with permission from American Chemical Society, © 2003 American Chemical Society.

$\gamma_{AS}$  and  $\gamma_{BS}$  have different prefactors in square brackets.

Based on the free energies given earlier, eqs 20 and 21, a phase diagram can be constructed in the phase space of three variables: the surface and lamellar inverse periodicities  $q_s$  and  $q_0$ , respectively, and the surface amplitude  $R$ . Three cuts in the phase diagram are given in Figure 10. In (a),  $R$  and  $q_s$  are scaled by  $q_0$ . An increase in  $q_s$  while keeping  $q_0$  and  $R$  constant generally leads to a preference of parallel layering. A different view is presented in (b), where  $q_0$  and  $R$  are scaled by  $q_s$ . Here, keeping  $q_s$  and  $q_0$  fixed while increasing  $R$  leads to a preference of perpendicular ordering. Similarly, in (c),  $R$  is used to scale  $q_s$  and

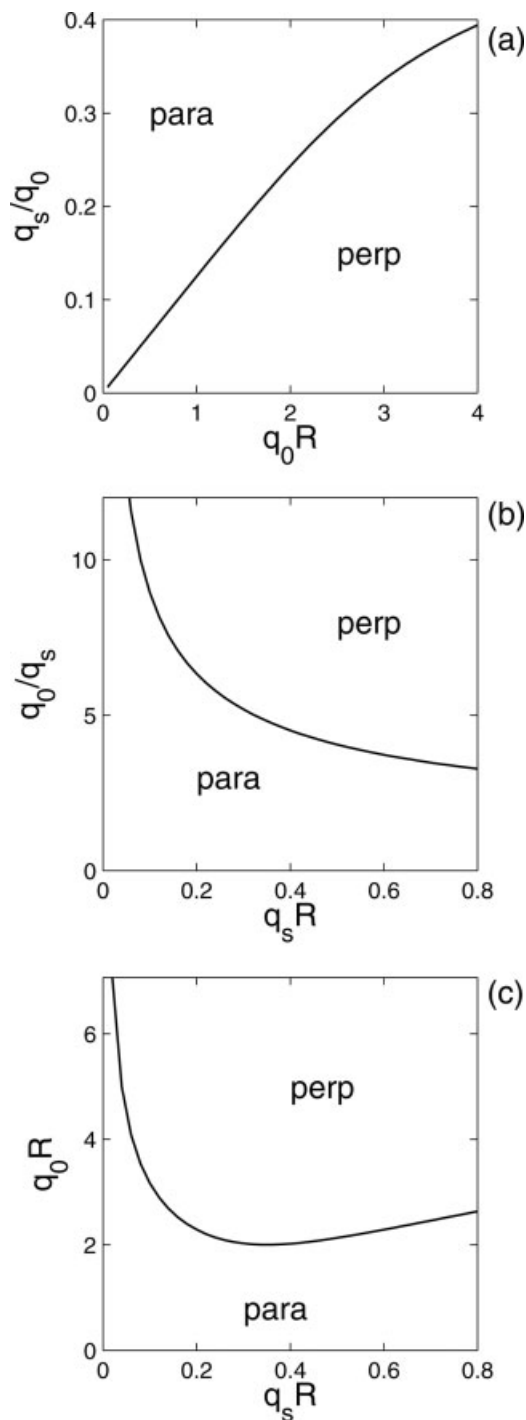


**Figure 10.** Phase diagrams for perpendicular and parallel lamellar on rough substrates. (a)  $R$  and  $q_s$  are scaled by  $q_0$ . (b) The surface wavenumber  $q_s$  is used to scale  $q_0$  and  $R$ . (c)  $q_s$  and  $q_0$  are scaled by the surface amplitude  $R$ . In the three plots we used  $\phi_0 = 0.4$ . The parameters used are  $\sigma = \gamma_{AS} - \gamma_{BS} = 0.25$  mN/m and  $\gamma_{AB} = 1$  mN/m. Reproduced from Tsori, Y.; Sivaniah, E.; Andelman, D.; Hashimoto, T. *Macromolecules* 2005, 38, 7193, with permission from American Chemical Society, © 2005 American Chemical Society.

$q_0$ . An increase of  $q_0$  at constant  $q_s$  and  $R$  favors perpendicular lamellae.

In the preceding sections, we have considered ordering mechanisms where the interaction of the polymers with the confining surfaces is mediated to regions far from the surfaces because of chain connectivity. We now turn to discuss orientation of BCP films in the presence of external electric fields. This is a bulk ordering mechanism that does not originate from the surface.

## BCPs IN PRESENCE OF ELECTRIC FIELDS

The influence that an electric field has on anisotropic polarizable media (e.g., BCP) is of great importance. We will, in particular, concentrate on two aspects: orientational transitions and order-to-order phase transitions.

### Orientation of Anisotropic Phases by an Electric Field

When a material with inhomogeneous dielectric constant is placed in an electric field  $E$ , there is an electrostatic free energy penalty for having dielectric interfaces perpendicular to the field.<sup>11,48–54</sup> This is the so-called “dielectric mechanism” for BCP orientation. Thus, a state where  $\nabla\epsilon$  is perpendicular to the field  $\mathbf{E}$  is favored.<sup>55–57</sup> The strength of this effect is proportional to  $(\epsilon_A - \epsilon_B)^2 E^2$ , where  $\epsilon_A$  and  $\epsilon_B$  are the dielectric constants of the polymers, and is enhanced when the difference in polarizabilities is large.

Consider BCP in the lamellar phase and confined between two flat and parallel electrodes. The lamellae may order parallel to the surfaces and suffer some unfavorable stretching or compression, in order to gain better surface coverage, as is discussed in the preceding sections. An applied electric field perpendicular to the surface will tend to orient the lamellae parallel to it, provided that it can overcome the interfacial interactions. In the weak-segregation regime ( $\phi \ll 1$ ), the electrostatic energy per unit volume is given by the Amundson–Helfand approximation.<sup>49,50</sup>

$$F_{\text{es}} = \frac{(\epsilon_A - \epsilon_B)^2}{2\bar{\epsilon}} \sum_{\mathbf{q}} (\hat{\mathbf{q}} \cdot \mathbf{E})^2 \phi_{\mathbf{q}}^2 \quad (22)$$

where the sum is taken over all  $q$ -modes in the expression  $\phi(\mathbf{r}) = \sum_{\mathbf{q}} \phi_{\mathbf{q}} \cos(\mathbf{q} \cdot \mathbf{r})$ , and  $\bar{\epsilon} = f\epsilon_A + (1-f)\epsilon_B$  is the average dielectric constant.

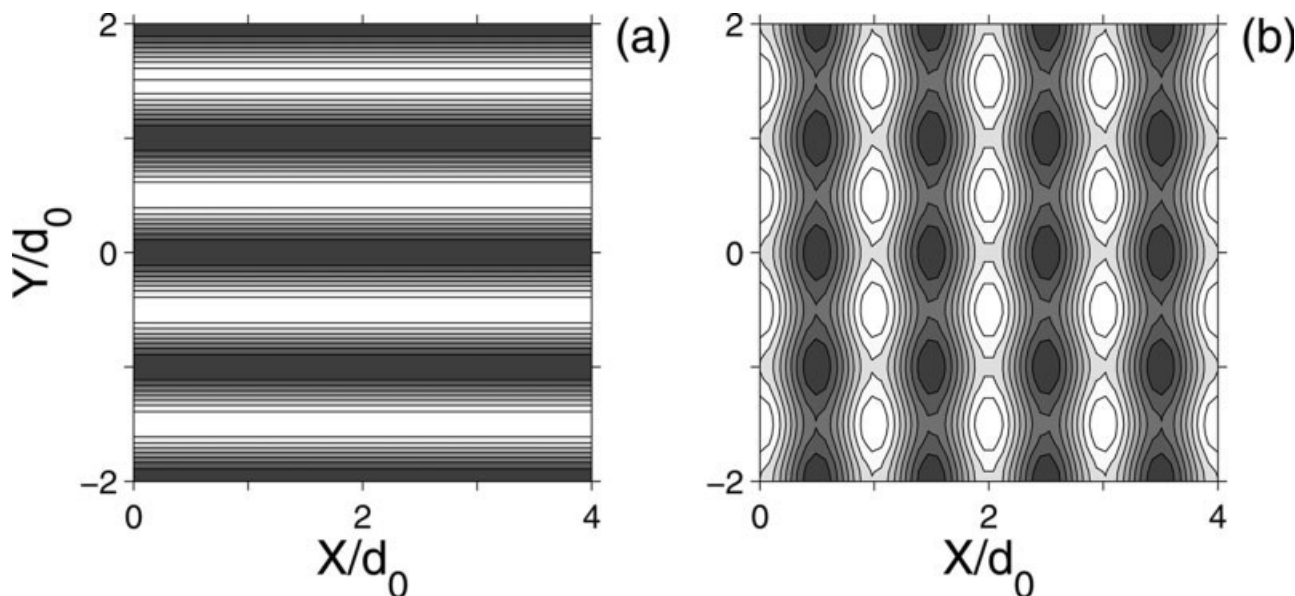


**Figure 11.** BCP lamellar layers between two surfaces and under external electric field. The surfaces are at  $y = \pm 2d_0$ , and the field is in the  $y$  direction. The B monomers (colored black) are attracted to both surfaces. (a) The field is slightly smaller than the critical field,  $E = 0.98E_c$ , and the film has a perfect parallel ordering. (b) The field is just above the threshold,  $E = 1.02E_c$ . The film morphology is a superposition of parallel and perpendicular lamellae. Reproduced from Tsori, Y.; Andelman, D. *Macromolecules* 2002, 35, 5161, with permission from American Chemical Society, © 2002 American Chemical Society.

A proper *ansatz* for the copolymer morphology is a linear combination of parallel and perpendicular layering:  $\phi(\mathbf{r}) = w(\mathbf{E})\phi_{\parallel}(\mathbf{r}) + g(\mathbf{E})\phi_{\perp}(\mathbf{r})$ , with field-dependent amplitudes  $w(\mathbf{E})$  and  $g(\mathbf{E})$ . When this *ansatz* is substituted into the free-energy eq 22, the amplitudes can be calculated and the order parameter is obtained.

Figure 11 shows the resulting BCP morphology under external electric field oriented perpendicular to the surfaces.<sup>48</sup> In (a) the field is just below a *critical field* and the lamellae lie parallel to the electrodes. However, when the field is increased just above the critical field, a transition occurs to a highly distorted but predominantly perpendicular layering [see (b)]. As the field further increases, the modulations diminish and the lamellae achieve perfect ordering perpendicular to the surfaces.

In Figure 11(b), it is clear that the surface effect propagates far into the bulk, as the copolymer modulations persist throughout the whole film. In the strong-segregation regime, however, this is not true, and the surface effect is localized. We thus can imagine a third morphology, that of a “mixed” phase. In this morphology few parallel lamellae exist near the surfaces, while the rest of the film

is in the perpendicular orientation. A “T-junction” defect is therefore created, and a surface-tension term  $\gamma_T$  must be associated with it. Indeed such a morphology has been visualized lately by Russell and coworkers.<sup>58</sup>

The phase diagram in the plane of  $\delta$  and  $E$  is shown in Figure 12(a), where  $\delta \equiv (\gamma_{AS} - \gamma_{BS})/\gamma_T$ , for fixed surface separation.<sup>48</sup> There exist three fields  $E_1$ ,  $E_2$  and  $E_3$  separating the parallel, perpendicular, and mixed orientations. At small fields, there is a direct transition from parallel to perpendicular layers as the field is increased. The mixed state is only possible above a certain threshold of  $\delta$ ,  $\delta^*$ . Above this threshold, the mixed state is stable at fields larger than  $E_1$  but smaller than  $E_2$ . An increase of  $E$  above  $E_2$  leads to the stability of perpendicular lamellae.

The phase diagram in the  $L$  and  $E$  plane is shown in Figure 12(b), for a fixed value of  $\delta$ . At small surface separations, an increase of  $E$  leads to a transition from parallel to perpendicular lamellae at  $E = E_3$ . At surface separations larger than a threshold value  $L^*$ , increase of  $E$  above  $E_1$  leads to a mixed morphology, whereas further increase above  $E_2$  gives rise to perpendicular lamellae.

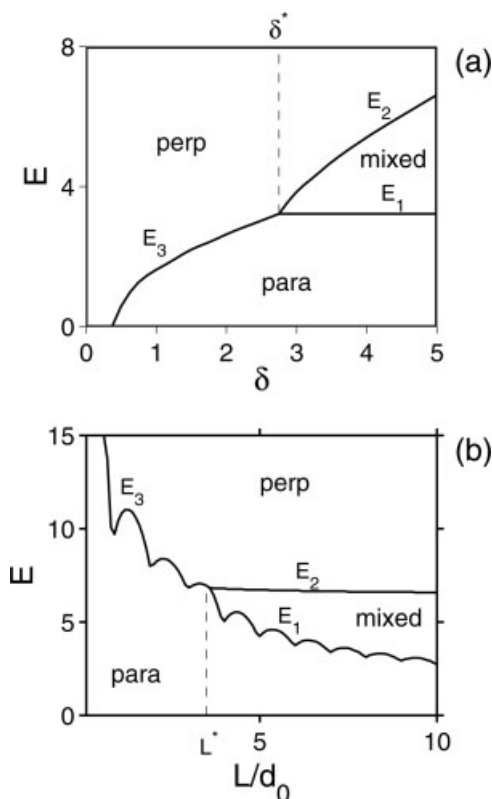


**Figure 12.** (a) Phase diagram in the  $E$ - $\delta$  plane. When  $\delta = (\sigma_{AS} - \sigma_{BS})/\gamma_T < \delta^*$ , there is a transition between parallel and perpendicular lamellae at  $E = E_3$ . At larger  $\delta$ ,  $\delta > \delta^*$ , the transition to the mixed state is followed by a second transition to the perpendicular state when  $E = E_2$ . The surface separation is chosen as  $L = 10d_0$ . (b) Similar diagram, but in the  $E$ - $L$  plane, with  $\delta = 5$ . Reproduced from Tsori, Y.; Andelman, D. *Macromolecules* 2002, 35, 5161, with permission from American Chemical Society, © 2002 American Chemical Society.

### Phase Transitions in Electric Fields

Orientation of anisotropic phases occurs when the ordered phase has some freedom to rotate, and when the applied electric fields are not too high. However, electric fields can cause a phase transition in systems composed of several components with different dielectric constants.<sup>59</sup> If the BCP phase under consideration cannot rotate in order to reduce the electrostatic energy, it begins to deform. A gradual change then occurs—this is usually an elongation of domain in the direction parallel to the field. At a certain point, it is more favorable for the system to make a drastic change in symmetry and “jump” to the state with the best (i.e. minimal) electrostatic energy.<sup>59,60</sup> This kind of phase transition is expected to occur at relatively high fields for BCPs,  $E \sim 50 - 100 \text{ V}/\mu\text{m}$ , so

sometimes the phase transition is preempted by dielectric breakdown of the material.

As an example of such a phase transition, consider diblock copolymers in the bcc phase of spheres, under an electric field  $\mathbf{E}$ . To the lowest (quadratic) order in  $\phi$ , the electrostatic energy is given by the Amundson–Helfand expression eq 22. Higher order expressions are available as well.<sup>61</sup> At very high fields, the spheres will elongate into cylinder oriented along the field, which can be assumed to lie in the (1, 1, 1) direction of the lattice. The transition from perfect bcc to hexagonal symmetries of  $\phi$  can be achieved by the following *ansatz*:<sup>60</sup>

$$\phi(\mathbf{r}, \mathbf{E}) = w(\mathbf{E}) \sum_{n=1}^3 \cos(\mathbf{q}_n \cdot \mathbf{r}) + g(\mathbf{E}) \sum_{m=4}^6 \cos(\mathbf{q}_m \cdot \mathbf{r}) \quad (23)$$

where

$$\begin{aligned} \mathbf{q}_{1,4} &= q_0(\mp 1, 0, 1)/\sqrt{2} \\ \mathbf{q}_{2,5} &= q_0(1, \mp 1, 0)/\sqrt{2} \\ \mathbf{q}_{3,6} &= q_0(0, 1, \mp 1)/\sqrt{2} \end{aligned} \quad (24)$$

At zero electric field,  $w(\mathbf{E}) = g(\mathbf{E})$  and  $\phi$  represents a bcc phase. For large enough field, the order parameter reduces to the hexagonal one:  $g(\mathbf{E}) = 0$ , and  $\phi_{\text{hex}}(\mathbf{r}) = A_{\text{hex}} \sum_{n=1}^3 \cos(\mathbf{q}_n \cdot \mathbf{r})$ .

The result of the minimization of  $F = F_b + F_{\text{es}}$  gives the value of  $w(\mathbf{E})$  and  $g(\mathbf{E})$  and therefore  $\phi$ . Figure 13(a) shows the BCP morphology in the absence of field. As the field is increased, the spheres deform and elongate along the external field. This state represents a compromise between electrostatic energy and stretching of the polymer chains. There exist a critical field  $E_c$  above which a direct transition to cylinders occurs: in (b) the field is  $E = 0.98E_c$ , while in (c) the field is just above the critical one ( $E = 1.02E_c$ ), and perfect cylinders are formed.

The complete phase diagram, taking into account the relative stability of the various mesophases, can be calculated. We have done so by two mean-field methods: the first is an analytical method based on the earlier coarse-graining approach. The second one is a more rigorous treatment based on numerical solutions of self-consistent field equations for the copolymer concentration.<sup>61</sup> The result is shown in Figure 14 in the plane of field  $E$  and Flory parameter  $\chi$ , and for

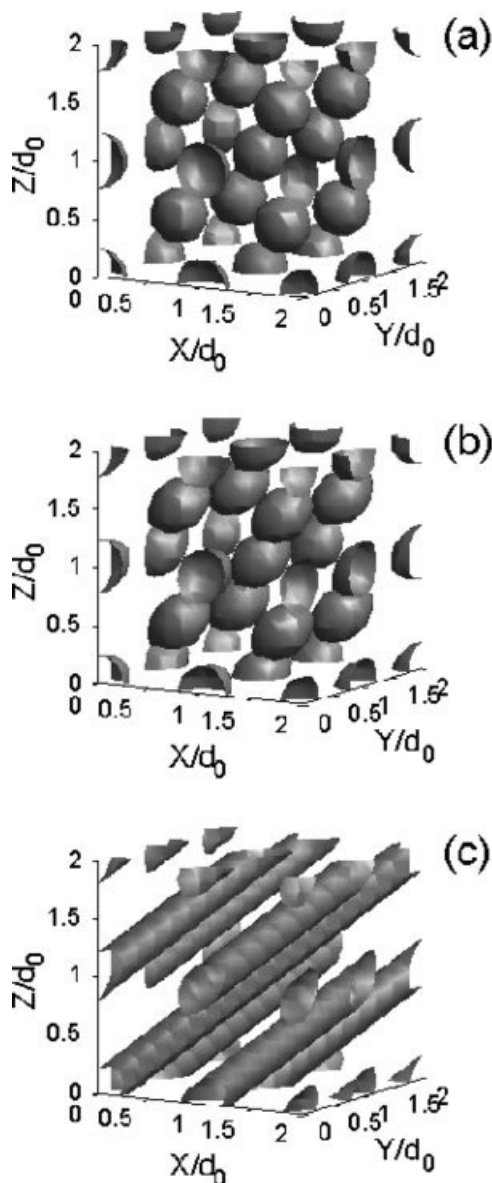


**Figure 13.** Cubic phase of BCP in electric field. (a) Electric field is  $E = 0$ . (b)  $E = 0.98E_c$ , just 2% below the critical field, and oriented along the (1, 1, 1) direction of the lattice. The spheres are deformed. (c)  $E = 1.02E_c$ , just above the critical field, and the system undergoes an abrupt change into the hexagonal array of cylinders. Reproduced from Tsori, Y.; Tournilhac, F.; Andelman, D.; Leibler, L. *Phys Rev Lett* 2003, 90, 145504, with permission from American Physical Society.

a particular composition  $f = 0.3$ . The distorted bcc phases, denoted as  $R\bar{3}m$ , is bounded by the hexagonal (hex) and disordered (dis) phases. All three meet at a triple point  $(E_t, \chi_t) = (0.49, 14.11/N)$ , where fields are scaled by  $\hat{E}_0 \equiv (\epsilon_0 v_p / k_B T)^{-1/2}$ , where  $\epsilon_0$  is the vacuum permittivity and  $v_p$  is the volume of one copolymer chain.

### Ionic Impurities in BCPs

The earlier discussion pertains to somewhat “ideal” polymers, because, in the electric response, only their dielectric constant was considered. However, most polymers are prepared by anionic polymerization. The process is initiated by one butyl-lithium ion (BuLi). After rinsing with water, the loose Li binds with an OH group to form LiOH, some of which are dissociated. Hence, there is a finite number of positive and negative ions in the material, and their presence changes the system behavior.

The existence of dissociated ions means that there are additional forces which act in the alignment process of the BCP mesophases. These forces depend on the mobility  $\mu$  of the ions, and on the frequency  $\omega$  of applied field. The torque due to mobile ions is expected to be large if the drift velocity  $\pi e \mu E / \omega$  is larger than the BCP domain size,  $d_0$ . In addition, mobile charges also mean that there is dissipation. Hence, the energy stored in the dielectric medium  $\epsilon E^2$  should be compared to the Joule heating in one cycle of the field  $2\pi\sigma E^2 / \omega$ , where  $\sigma$  is the ions conductivity, proportional to the ion density. It is clear from the aforementioned fact

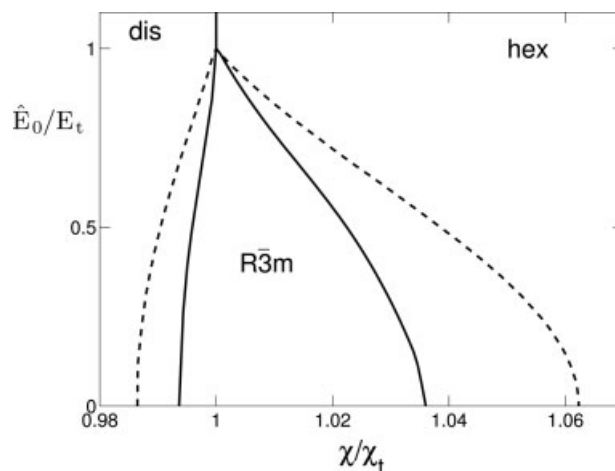


**Figure 14.** Phase diagram of BCPs in electric field, in the plane of the Flory parameter  $\chi$  and normalized electric field  $\hat{E}_0$ . The distorted bcc phase, denoted as  $R\bar{3}m$ , is bounded by the hexagonal (hex) and disordered (dis) phases. Solid line is the prediction of analytical one-mode approximation, whereas dashed lines are obtained by a more accurate self-consistent numerical study. Axes are scaled by  $(\chi_t, E_t)$ , the values of  $\chi$  and  $\hat{E}_0$  at the triple point. Reproduced from Tsori, Y.; Andelman, D.; Lin, C.-Y.; Schick, M. *Macromolecules* 2003, 36, 5873, with permission from American Chemical Society, © 2003 American Chemical Society.

that, for low frequencies (in practice  $\lesssim 100$  Hz), mobile-dissociated ions begin to play an important role in BCP alignment and phase transitions.<sup>62</sup>

When the additional complexity due to these ions is taken into account, it turns out that the orientation forces (torques) due to the mobile ions scale as  $1/\omega$ ,<sup>62</sup> and are equal to the ones due to the regular “dielectric mechanism” at about 50 Hz. Consequently, they are twice as large at 25 Hz, and they become more important as the frequency is reduced.

Taking into account the effect of mobile ions on the BCP phase transition, as outlined earlier (from bcc phase of spheres to a hexagonal array of cylinders), it turns out that the transition field  $E_c$  can be significantly reduced from a value of  $\approx 70\text{--}100$  V/ $\mu\text{m}$  to values  $\sim 20$  V/ $\mu\text{m}$ .<sup>60</sup>

## CONCLUSIONS

We review in this paper several ordering mechanisms in confined BCPs. The theoretical approach relies on a mean-field coarse-grained Hamiltonian, which is less sensitive to microscopic details and valid for a wide class of systems showing self-assembly in soft-matter. This approach thus complements other computationally-intensive self-consistent numerical schemes<sup>34–36,63,64</sup> and Monte-Carlo simulations.<sup>65–68</sup> The polymer density near a chemically patterned surface is given above the order–disorder temperature as a function of the surface pattern. In this regime, the chemical pattern  $q$ -modes give rise to density modes which are decoupled from each other (linear response theory). In the weak segregation regime, the surface correlations are long range and, therefore, simple chemical patterns yield complex copolymer morphology, even though the bulk is in its disordered phase.

Below the ODT temperature, we consider lamellae confined by homogeneous surfaces, and examine the relative stability of parallel *vs.* perpendicular ordering as a function of temperature, surface separation, and interfacial interactions. Lamellae confined by striped surface, whose periodicity is larger than the lamellar periodicity, appear tilted with respect to the surface thereby optimizing their surface interactions. The lamellar undulations are more prominent as the ODT is approached. Mixed lamellar phases appear when one surface has chemically patterns in the form of stripes while the other is uniform.

A different paradigm for control of BCP orientation in thin films is using rough surfaces. This method may be advantageous over other methods in several situations, since it is relatively simple to implement experimentally. The phase diagram is presented for the ordered phases as a function of surface period, surface amplitude, and lamellar period, as well as other parameters.

Lastly, the influence of electric field on the phase behavior of BCPs is considered. An external electric field favors a state where dielectric interfaces are parallel to the field itself. Hence, from an electrostatic viewpoint, lamellae confined in a thin film are preferentially oriented perpendicular rather than parallel to the confining electrodes. In the weak-segregation regime, there is one critical field at which parallel layers are transformed into perpendicular ones. Even for fields larger than the critical field, the long-range effect of the surfaces is evident as strong lamellar undulations. The strong segregation regime is considered as well. Here we find three possible states: parallel, perpendicular, and mixed. The last morphology exhibits few parallel layers close to the electrodes while the rest of the film is perpendicular. There are either two or one critical fields separating them, depending on the interfacial interactions.

An electric field can also bring about phase transitions in ordered phases by means of minimizing dielectric interfaces perpendicular to the field direction. The transition from the bcc phase of spheres to a hexagonal array of cylinders under the influence of electric field is discussed as an example. Below the critical field, the spheres elongate in the field’s direction, but above it we find perfect cylinder whose axes are parallel to the field. The phase diagram of the various mesophases is calculated, and the simple analytical expression obtained with the coarse-graining theory is compared with a more rigorous SCF theory, with rather good match. We point out that residual dissociated ions in BCPs can greatly enhance the electric field effect, and this is especially true in low-frequency electric fields.

The analytical calculations presented here rely on a relatively simple mean-field coarse-grained free-energy functional. This approach allowed us to deal with confinement effects in BCP, take into account the chemical nature of the surfaces, calculate the elastic energy penalty and lamellar conformation near curved interfaces, and balance the electrostatic energy against the elastic one for BCPs in electric fields. The coarse-grained approach has a big advantage that it can be

generalized and account for other complex polymer systems. Because it is less accurate in terms of quantitative predictions, it is useful to compare this approach with numerical self-consistent field theories, discrete lattice models, Monte-Carlo, and molecular dynamic simulations and experiments.

Our research on block copolymer has been conducted in collaboration with T. Hashimoto, L. Leibler, C.-Y. Lin, M. Schick, E. Sivaniah, and F. Tournilhac. We thank K. Binder, Y. Cohen, G. Fredrickson, S. Gido, G. Krausch, M. Muthukumar, T. Ohta, G. Reiter, T. P. Russell, U. Steiner, I. Szleifer, E. L. Thomas, T. Thurn-Albrecht, M. Turner, and T. Xu for numerous discussions. This research is partly supported by the Israel Science Foundation (ISF) grants Nos. 160/05 (DA) and 284/05 (YT) and the US-Israel Binational Foundation (BSF) under grant No. 287/02.

## REFERENCES AND NOTES

- Hamley, I. W. *The Physics of Block Copolymers*; Oxford University press: Oxford, 1998.
- Bates, F. S.; Fredrickson, G. H. *Phys Today* 1999, 52, 32.
- Cohen, Y.; Albalak, R. J.; Dair, B. J.; Capel, M. S.; Thomas, E. L. *Macromolecules* 2000, 33, 6502.
- Cohen, Y.; Brinkmann, M.; Thomas, E. L. *J Chem Phys* 2001, 114, 984.
- Chen, Z.-R.; Kornfield, J. A.; Smith, S. D.; Grothaus, J. T.; Satkowski, M. M. *Science* 1997, 277, 1248.
- Vlasov, Y. A.; Bo, X. Z.; Sturm, J. C.; Norris, D. J. *Nature* 2001, 414, 289.
- Fink, Y.; Winn, J. N.; Fan, S.; Chen, C.; Michel, J.; Joannopoulos, J. D.; Thomas, E. L. *Science* 1998, 282, 1679.
- Khandpur, A. K.; Foerster, S.; Bates, F. S.; Hamley, I. W.; Ryan, A. J.; Bras, W.; Almdal, K.; Mortensen, K. *Macromolecules* 1995, 28, 8796.
- Park, M.; Harrison, C.; Chaikin, P. M.; Register, R. A.; Adamson, D. H. *Science* 1997, 276, 1401.
- Thurn-Albrecht, T.; Schotter, J.; Kästle, G. A.; Emley, N.; Shibauch, T.; Krustin-Elbaum, L.; Guarini, K.; Black, C. T.; Tuominen, M. T.; Russell, T. P. *Science* 2000, 290, 2126.
- Ashok, B.; Muthukumar, M.; Russell, T. P. *J Chem Phys* 2001, 115, 1559.
- Park, C.; Yoon, J.; Thomas, E. L. *Polymer* 2003, 44, 6725.
- Bucknall, D. G. *Prog Mat Sci* 2004, 49, 713.
- Leibler, L. *Macromolecules* 1980, 13, 1602.
- Binder, K.; Frisch, H. L.; Stepanow, S. *J Phys II* 1997, 7, 1353.
- Petera, D.; Muthukumar, M. *J Chem Phys* 1997, 107, 9640.
- Petera, D.; Muthukumar, M. *J Chem Phys* 1998, 109, 5101.
- Fredrickson, G. H.; Helfand, E. *J Chem Phys* 1987, 87, 697.
- Ohta, T.; Kawasaki, K. *Macromolecules*, 1986, 19, 2621.
- Tsori, Y.; Andelman, D. *Europhys Lett* 2001, 53, 722.
- Brown, G.; Chakrabarty, A. *J Chem Phys* 1994, 101, 3310.
- Brown, G.; Chakrabarty, A. *J Chem Phys* 1995, 102, 1440.
- Swift, J.; Hohenberg, P. C. *Phys Rev A* 1997, 15, 319.
- Bates F. S.; Fredrickson, G. H. *Annu Rev Phys Chem* 1990, 41, 525.
- Brazovskii, S. A. *Sov Phys JETP* 1975, 41, 85.
- Kellogg, G. J.; Walton, D. G.; Mayes A. M.; Lambooy, P.; Russell, T. P.; Gallagher P. D.; Satija, S. K. *Phys Rev Lett* 1996, 76, 2503.
- Mansky, P.; Russell, T. P.; Hawker, C. J.; Mayes, J.; Cook, D. C.; Satija, S. K. *Phys Rev Lett* 1997, 79, 237.
- Tsori, Y.; Andelman, D. *Interface Sci* 2003, 11, 259.
- Tsori, Y.; Andelman, D. *Macromolecules* 2001, 34, 2719.
- Tsori, Y.; Andelman, D.; Schick, M. *Phys Rev E* 2000, 61, 2848.
- Walton, D. G.; Kellogg, G. J.; Mayes, A. M.; Lambooy, P.; Russell, T. P. *Macromolecules* 1994, 27, 6225.
- Fredrickson, G. H. *Macromolecules* 1987, 20, 2535.
- Turner, M. S. *Phys Rev Lett* 1992, 69, 1788.
- Matsen, M. W. *J Chem Phys* 1997, 106, 7781.
- Matsen, M. W.; Bates, F. S. *J Chem Phys* 1997, 106, 2436.
- Pickett, G. T.; Balazs, A. C. *Macromolecules* 1997, 30, 3097.
- Geisinger, T.; Mueller, M.; Binder, K. *J Chem Phys* 1999, 111, 5241.
- Wang, Q.; Yan, Q.; Nealey, P. F.; de Pablo, J. J. *J Chem Phys* 2000, 112, 450.
- (a) Pereira, G. G.; Williams, D. R. M. *Macromolecules* 1999, 32, 1661; (b) Pereira, G. G.; Williams, D. R. M. *Macromolecules* 1999, 32, 758.
- Wang, Q.; Nath, S. K.; Graham, M. D.; Nealey P. F.; de Pablo, J. J. *J Chem Phys* 2000, 112, 9996.
- Tsori, Y.; Andelman, D. *Eur Phys J E* 2001, 5, 605.
- Heier, J.; Kramer, E. J.; Walheim, S.; Krausch, G. *Macromolecules* 1997, 30, 6610.
- Tsori, Y.; Andelman, D. *J Chem Phys* 2001, 115, 1970.
- Tsori, Y.; Andelman, D. *Macromolecules* 2003, 36, 8560.
- Tsori, Y.; Sivaniah, E.; Andelman, D.; Hashimoto, T. *Macromolecules* 2005, 38, 7193.
- Turner, M. S.; Joanny, J.-F. *Macromolecules* 1992, 25, 6681.
- de Gennes, P.-G.; Prost, J. *The Physics of Liquid Crystals*, 2nd ed.; Oxford University Press: Oxford, 1993.
- Tsori, Y.; Andelman, D. *Macromolecules* 2002, 35, 5161.

49. Amundson, A.; Helfand, E.; Quan, X.; Smith, S. D. *Macromolecules* 1993, 26, 2698.
50. Amundson, K.; Helfand, E.; Quan, X.; Hudson, S. D.; Smith, S. D. *Macromolecules* 1994, 27, 6559.
51. Onuki, A.; Fukuda, J. *Macromolecules* 1995, 28, 8788.
52. Pereira, G. G.; Williams, D. R. M. *Macromolecules* 1999, 32, 8115.
53. Thurn-Albrecht, T.; DeRouchey, J.; Russell, T. P. *Macromolecules* 2000, 33, 3250.
54. Korylyuk, A. V.; Zvelindovsky, A. V.; Sevink, G. J. A.; Fraaije, J. G. E. M. *Macromolecules* 2002, 35, 1473.
55. Böker, A.; Knoll, A.; Elbs, H.; Abetz, V.; Müller, A. H. E.; Krausch, G. *Macromolecules* 2002, 35, 1319.
56. Böker, A.; Schmidt, K.; Knoll, A.; Zettl, H.; Hansel, H.; Urban, V.; Abetz, V.; Krausch, G. *Polymer* 2006, 47, 849.
57. Böker, A.; Elbs, H.; Hansel, H.; Knoll, A.; Ludwigs, S.; Zettl, H.; Zvelindovsky, A. V.; Sevink, G. J. A.; Urban, V.; Abetz, V.; Müller, A. H. E.; Krausch, G. *Macromolecules* 2003, 36, 8078.
58. Xu, T.; Hawker, C. J.; Russell, T. P. *Macromolecules* 2005, 38, 2802.
59. Tsori, Y.; Tournilhac, F.; Leibler, L. *Nature* 2004, 430, 544.
60. Tsori, Y.; Tournilhac, F.; Andelman, D.; Leibler, L. *Phys Rev Lett* 2003, 90, 145504.
61. Tsori, Y.; Andelman, D.; Lin, C.-Y.; Schick, M. *Macromolecules* 2006, 39, 289.
62. Tsori, Y.; Tournilhac, F.; Leibler, L. *Macromolecules* 2003, 36, 5873.
63. Shull, K. R. *Macromolecules* 1992, 25, 2122.
64. Matsen, M. W.; Schick, M. *Phys Rev Lett* 1994, 72, 2660.
65. Binder, K. *Acta Polym* 1995, 46, 204.
66. Binder, K. *Top Appl Phys* 1995, 71, 355.
67. Szleifer, I.; Loring, R. F. *J Chem Phys* 1994, 100, 5367.
68. Szleifer, I. *Curr Opin Colloid Sci* 1996, 1, 416.